Inorg. Chem. **2002**, *41*, 5241–5248

Ion Pair Charge-Transfer Complexes between Anionic and Cationic Metal-Dithiolenes [M(II) = Pd, Pt]

Francesco Bigoli,[†] Paola Deplano,*[,‡] Maria Laura Mercuri,[‡] Maria Angela Pellinghelli,[†] Luca Pilia,[‡] Gloria Pintus,[‡] Angela Serpe,[‡] and Emanuele F. Trogu[‡]

Dipartimento di Chimica Generale ed Inorganica, Chimica Analitica, Chimica Fisica, Università di Parma, Parco Area delle Scienze 17A, I-43100 Parma, Italy, and Dipartimento di Chimica Inorganica ed Analitica, Università di Cagliari, Cittadella di Monserrato, I-09042 Monserrato, Cagliari, Italy

Received June 12, 2002

New $[M(R_2pipdt)_2](BF_4)_2$ salts [R_2pipdt = *N*,*N*′-dialkyl-piperazine-2,3-dithione; M = Pd(II), R = Me and M = Pt(II), R = Me, Et, Pr^i] bearing redox-active cationic dithiolene complexes have been prepared and characterized. These cations react with the redox-active $[M(mnt)_2]^{2-}$ [M = Pd(II), Pt(II); mnt = maleonitrile-2,3-dithiolate] anionic dithiolenes to form salts describable as ion pair charge-transfer complexes. X-ray crystallographic studies have shown that $[M(Me_2pipdt)_2][M(mnt)_2]$ complexes, with M = Pd(II) and Pt(II), are isomorphous. Crystal data of the Pt salt (**3a**): triclinic, $P\bar{1}$ (No. 2); $Z = 1$; $T = 293(2)$ K; $a = 6.784(7)$ Å, $b = 8.460(6)$ Å, $c = 13.510(5)$ Å, $\alpha = 100.63(2)°$, $\beta = 104.04(2)°$, $\gamma = 96.90(2)°$; R1 = 0.0691 [wR2 = 0.2187 (all data)]. Structural data show that approximately square-planar $[Pt(Me_2pipdt)_2]$ dications and regular square-planar $[Pt(mnt)_2]$ dianions form an infinite anion–cation one-dimensional stack along axis *a* with a Pt···Pt *a*/2 distance of 3.392 Å and a Pt···Pt···Pt angle of 180°. Anions and cations arrange themselves face-to-face so as to take on a staggered arrangement. These salts exhibit strong absorptions in the visible–near-infrared region assigned to ion pair charge-transfer transitions. A relation between the optical and thermal electron transfer in the solid state is obtained using a "Marcus–Hush model", and a solid-state electrical conductivity in agreement with expectations is observed. Vibrational spectroscopy is in agreement with the existence of charge-transfer interactions between the cationic and anionic components of the salts.

Introduction

The present interest in metal-dithiolene complexes is due to their applications in the areas of conducting[1] and magnetic materials,[2] near-infrared dyes,[3] and nonlinear optical materials.[4] Neutral square-planar metal-dithiolenes (Ni, Pd, Pt) are 16-electron metal complexes with a 14-π-electron system. Early semiempirical and more sophisticated recent theoretical studies have been carried out on these complexes.[5] The HOMO and LUMO are delocalized over both ligands, and the electronic transition between these orbitals gives rise to a strong absorption in the near-infrared region, which makes these complexes suitable to be used as near-infrared dyes. Donor substituents in the parent dithiolene $[Ni(edt)_2]$ (edt = ethylenedithiolate) raise the energy of the HOMO more than that of the LUMO, producing a shift of the low-energy band to lower frequencies. This is desirable for obtaining dyes to be applied for Q-switching infrared lasers,[6] but strong donor substituents can also force the HOMO to become antibonding with an undesirable induced increased reactivity leading to the loss of one or two electrons. However, cationic dithiolenes are rare and generally obtained through irreversible

* To whom correspondence should be addressed. E-mail: deplano@vaxca1.unica.it. Phone: (+39) 070 675 4680. Fax: (+39) 070 675 4499.
† Università di Parma.
‡ Università di Cagliari.

(1) Cassoux, P.; Valade, L. *Inorganic Materials*, 2nd ed.; Bruce, D. W., O'Hare, D., Eds.; John Wiley & Sons: Chichester, U.K., 1996. Tanaka, H.; Okano, Y.; Kobayashi, H.; Suzuki, W.; Kobayashi, A. *Science* **2001**, *291*, 285.
(2) Coomber, A. T.; Beljonne, D.; Friend, R. H.; Brédas, J. K.; Charlton, A.; Robertson, N.; Underhill, A. E.; Kurmoo, M.; Day, P. *Nature* **1996**, *380*, 144. Robertson, N.; Cronin, L. *Coord. Chem. Rev.* **2002**, *227*, 93.
(3) Mueller-Westerhoff, U. T.; Vance, B.; Yoon, D. I. *Tetrahedron* **1991**, *47*, 909.
(4) Winter, C. S.; Hill, C. A. S.; Underhill, A. E. *Appl. Phys. Lett.* **1991**, *58*, 107.
(5) Lauterbach, C.; Fabian, J. *Eur. J. Inorg. Chem.* **1999**, 1995. Aragoni, C.; Arca, M.; Demartin, F.; Devillanova, F. A.; Garau, A.; Isaia, F.; Lelj, F.; Lippolis, V.; Verani, G. *J. Am. Chem. Soc.* **1999**, *121*, 7098.
(6) Herman, Z. S.; Kirchner, R. F.; Loew, G. H.; Mueller-Westerhoff, U. T.; Nazal, A.; Zerner, M. C. *Inorg. Chem.* **1982**, *21*, 46. Mueller-Westerhoff, U. T. *Comprehensive Coordination Chemistry*; Wilkinson, G., Ed.; Pergamon Press: Oxford, 1987.

10.1021/ic025788w CCC: $22.00
Published on Web 09/13/2002

electrochemical oxidation.[7] Despite the presence of the strong N-donor atoms adjacent to the dithiolene core, a class of stable nickel-dithiolenes based on the ligand R_2timdt (formally the monoanion of 1,3-dialkylimidazolidine-2,4,5-trithione), showing promising properties for Q-switching neodymium lasers, has been prepared.[8] On the other hand, by using *N*,*N*′-dimethyl-piperazine-2,3-dithione (Me_2pipdt), where the N-donor atoms are similarly adjacent to the dithiolene moiety, but inserted into a hexa-atomic ring instead, the $[Ni(R_2pipdt)_2](BF_4)_2$ salts of dicationic dithiolenes have been obtained and characterized.[9] These complexes are valuable reagents for preparing mixed-ligand (or unsymmetrical) nickel-dithiolenes. In fact, by reacting $[Ni(R_2pipdt)_2](BF_4)_2$ with a salt of a nickel-dithiolene dianion such as $[Ni(mnt)_2]^{2-}$ (mnt = maleonitriledithiolate),[10] $[Ni(dmit)_2]^{2-}$ (dmit = 1,3-dithiole-2-thione-4,5-dithiolate),[11] or others, mixed-ligand derivatives have been obtained by a simple method in almost quantitative yields. These complexes are potential second-order nonlinear chromophores, because they are describable as dithione−dithiolate derivatives where the electronic transition between the HOMO, which possesses a prevailing contribution of the dithiolate ligand, and the LUMO, which possesses a prevailing contribution of the dithione ligand, has an intramolecular charge transfer (ICT) character,[12] which is required to generate β, the first molecular hyperpolarizability.[13] These complexes in fact show strong negative solvatochromism and β (a rough calculation based on the two-state model of NLO chromophores gave $\beta_0 = -130 \times 10^{-30}$ esu for [Ni(Pr^i_2-pipdt)(dmit)]).[9] Instead, the apparently similar unsymmetrical complexes [Ni(Pr^i_2timdt)(mnt)] and [Ni(Pr^i_2timdt)(dmit)][14] do not show CT transitions due to a strong delocalization involving both ligands. Accordingly, an approximately zero value of β has been determined for [Ni(Pr^i_2timdt)(mnt)].[9]

In this paper, we report the synthesis and characterization of palladium(II) and platinum(II) dicationic dithiolenes based on R_2pipdt ligands and their reactions with dithiolene metalates. Unlike the corresponding mixed-ligand nickel(II) complexes, this reaction produces double-salts with interesting solid-state properties. These salts, which consist of redox-active metal-dithiolene components, are describable as ion pair charge-transfer complexes exhibiting supramolecular CT interactions similar to those observed in salts of dianionic dithiolene metalates with dicationic redox-active organic donors such as 4,4′- and 2,2′-bipyridinium derivatives.[15]

Experimental Section

Reagents and solvents of reagent grade quality were used as supplied by Aldrich. The ligands R_2pipdt and the complexes $(Bu_4N)_2[M(mnt)_2]$ (M = Pt, Pd) were prepared according to refs 16 and 17.

Preparations. $[Pt(Me_2pipdt)_2](BF_4)_2$ (1a). Me_2pipdt (132 mg; 0.76 mmol) and $PtCl_2$ (100 mg; 0.38 mmol) (2:1 molar ratio) were mixed in CH_2Cl_2 (150 mL), in heterogeneous phase, and left under reflux for 24 h. The brown solution cleared, and a brown precipitate appeared. The solvent was rotary-evaporated and the crude product dissolved in EtOH giving a violet solution. The unreacted $PtCl_2$ was removed by filtration. The filtered solution was mixed with $NaBF_4$ (87 mg; 0.79 mmol) in EtOH. The crude brown product was collected by filtration and recrystallized by CH_3CN/Et_2O to give **1a** (yield 30%). Anal. Calcd for $C_{12}H_{20}N_4PtS_4B_2F_8$: C, 20.10; H, 2.81; N, 7.81; S, 17.88. Found: C, 20.43; H, 2.70; N, 7.85; S, 17.70%. IR [KBr pellets, cm^{-1}]: 2952w; 2855vw; 1550vs; 1432w; 1400m; 1368s; 1293m; 1265m; 1212w; 1149vs; 1061vs; 895w; 664vw; 538ms; 522m; 460w. Raman (cm^{-1}): 2923w; 1568vs; 1419m; 1374s; 1276s; 1151m; 545m; 413m; 155m; 93m. UV−vis (in CH_3CN), λ/nm (ϵ/dm^3 mol^{-1} cm^{-1}): 225 (35350); 369sh; 489sh; 516 (13300).

$[Pd(Me_2pipdt)_2](BF_4)_2$ (2a). This compound was prepared as described (yield 81%), starting from Me_2pipdt (197 mg; 1.13 mmol) and $PdCl_2$ (100 mg; 0.56 mmol) in CH_2Cl_2 (150 mL). Anal. Calcd for $C_{12}H_{20}N_4PdS_4B_2F_8$: C, 22.93; H, 3.21; N, 8.91; S, 20.40. Found: C, 22.38; H, 3.15; N, 8.61; S, 20.09%. IR [KBr pellets, cm^{-1}]: 3013vw; 1553vs; 1444w; 1409m; 1370vs; 1294s; 1213w; 1147vs; 1059vs; 891vw; 815vw; 685vw; 600vw; 538ms; 522m; 476vw. Raman (cm^{-1}): 2924w; 2822vw; 1568vs; 1440w; 1417w; 1373s; 1276m; 1151w; 766vw; 543w; 394vw; 147s; 86s. UV−vis (in CH_3CN), λ/nm (ϵ/dm^3 mol^{-1} cm^{-1}): 220 (31200); 287 (38800); 424 (13400); 450 (15200).

$[Pt(Et_2pipdt)_2](BF_4)_2$ (1b). This compound was prepared as described for **1a** (yield 97%), starting from Et_2pipdt (152 mg; 0.75 mmol) and $PtCl_2$ (100 mg; 0.38 mmol) in CH_2Cl_2 (150 mL). The crude product collected from the evaporated solution was dissolved in a MeOH/EtOH mixture. Anal. Calcd for $C_{16}H_{24}N_4PtS_4B_2F_8$: C, 24.85; H, 3.65; N, 7.24; S, 16.58. Found: C, 24.98; H, 3.89; N, 7.28; S, 17.47%. IR [KBr pellets, cm^{-1}]: 3100vw; 2974w; 2944w; 1617w; 1546vs; 1451m; 1369s; 1338m; 1305vw; 1280w; 1256w; 1229s; 1193w; 1139s; 1048vs; 985sh; 885vw; 858w; 793w; 769vw; 681w; 613w; 546m; 538sh; 521m. UV−vis (in CH_3CN), λ/nm (ϵ/dm^3 mol^{-1} cm^{-1}): 205 (28200); 231 (35100); 272sh; 375 (5400); 491 sh; 524 (20700); 584 sh.

$[Pt(Pr^i_2pipdt)_2](BF_4)_2$ (1c). This compound was prepared as described for **1a** (yield 37%), starting from Pr^i_2pipdt (173 mg; 0.75 mmol) and $PtCl_2$ (100 mg; 0.38 mmol) refluxed in CH_2Cl_2 (150

(7) Kushch, L. A.; Konovalikhin, S. V.; Buravov, L. I.; Khomenko, A. G.; Shilov, G. V.; Van, K.; Dyachenko, O. A.; Yagubskii, E. B.; Rovira, C.; Canadell, E. *J. Phys. I* **1996**, *6*, 1555 and references therein.

(8) Bigoli, F.; Deplano, P.; Devillanova, F. A.; Lippolis, V.; Lukes, P. J.; Mercuri, M. L.; Pellinghelli, M. A.; Trogu, E. F. *J. Chem. Soc., Chem. Commun.* **1995**, 371. Bigoli, F.; Deplano, P.; Devillanova, F. A.; Ferraro, J. R.; Lippolis, V.; Lukes, P. J.; Mercuri, M. L.; Pellinghelli, M. A.; Trogu, E. F.; Williams, J. M. *Inorg. Chem.* **1997**, *36*, 1218. Bigoli, F.; Deplano, P.; Mercuri, M. L.; Pellinghelli, M. A.; Pintus, G.; Trogu, E. F.; Zonnedda, G.; Wang, H. H.; Williams, J. M. *Inorg. Chim. Acta* **1998**, *273*, 175.

(9) Bigoli, F.; Chen, C.-T.; Deplano, P.; Mercuri, M. L.; Pellinghelli, M. A.; Pilia, L.; Pintus, G.; Trogu, E. F. *Chem. Commun.* **2001**, 2246.

(10) Billig, E.; Williams, R.; Bernal, I.; Waters, J. H.; Gray, H. B. *Inorg. Chem.* **1964**, *3*, 663.

(11) Steimecke, G.; Sieler, H. J.; Kirmse, R.; Hoyer, E. *Phosphorus Sulfur Relat. Elem.* **1979**, *7*, 49.

(12) Vogler, A.; Kunkely, H. *Angew. Chem., Int. Ed. Engl.* **1982**, *21*, 77.

(13) Kato, R.; Kashimura, Y.; Sawa, H.; Okano, Y. *Chem. Lett.* **1997**, 921. Chen, C.-T.; Liao, S.-Y.; Lin, K.-J.; Lai, L.-L. *Adv. Mater.* **1998**, *3*, 335.

(14) Bigoli, F.; Cassoux, P.; Deplano, P.; Mercuri, M. L.; Pellinghelli, M. A.; Pintus, G.; Serpe, A.; Trogu, E. F. *J. Chem. Soc., Dalton Trans.* **2000**, 4639−4644.

(15) Nunn, I.; Eisen, B.; Benedix, R.; Kisch, H. *Inorg. Chem.* **1994**, *33*, 5079−5085. Kisch, H. *Coord. Chem. Rev.* **1997**, *159*, 385−396. Kisch, H.; Eisen, B.; Dinnebier, R.; Shankland, K.; David, W. I. F.; Knoch, F. *Chem.—Eur. J.* **2001**, *7*, 738.

(16) Isaksson, R.; Liljefors, T.; Sandstrom, J. *J. Chem. Res., Miniprint* **1981**, 664.

(17) Billig, E.; Williams, R.; Bernal, I.; Waters, J. H.; Gray, H. B. *Inorg. Chem.* **1964**, *3*, 663 and references therein.

mL). Anal. Calcd for $C_{20}H_{36}N_4PtS_4B_2F_8$: C, 28.96; H, 4.37; N, 6.75; S, 15.46. Found: C, 29.16; H, 4.61; N, 6.69; S, 15.60%. IR [KBr pellets, cm^{-1}]: 2976w; 1611w; 1528vs; 1460w; 1366s; 1285w; 1237m; 1183m; 1113vs; 1061vs; 900w; 725vw; 600vw; 585m; 532vw; 522w. Raman (cm^{-1}): 1536vs; 1435w; 1368m; 1278w; 1239s; 1174vw; 900w; 482w; 392m; 142w; 81mw. UV−vis (in CH_3CN), λ/nm (ϵ/dm^3 mol^{-1} cm^{-1}): 209 (22100); 233 (27550); 267sh; 371 (4400); 496 sh; 521 (14850).

[Pt(Me$_2$pipdt)$_2$][Pt(mnt)$_2$] (3a). The brown CH_3CN solution (30 mL) of $[Pt(Me_2pipdt)_2](BF_4)_2$ (100 mg; 0.14 mmol) was slowly added to the warm orange CH_3CN solution (30 mL) of $(Bu_4N)_2$-$[Pt(mnt)_2]$ (133 mg; 0.14 mmol). The solution turned to violet, and a quantitative precipitation of brown needle-shaped crystals occurred (yield 99%). Crystals suitable for X-ray characterization were grown using a diffusion cell with three compartments connected through porous glass frits. The solutions of the components were introduced in the terminal compartments, and the crystals were collected in the central compartment filled with CH_3CN. Anal. Calcd for $C_{10}H_{10}N_4PtS_4$: C, 23.57; H, 1.98; N, 11.00; S, 25.17. Found: C, 24.00; H, 1.84; N, 11.08; S, 25.78%. IR [KBr pellets, cm^{-1}]: 3000vw; 2965vw; 2295vw; 2250vw; 2191vs; 1528vs; 1460vs; 1435vw; 1399s; 1355vs; 1289m; 1265m; 1204m; 1152m; 1143s; 1102s; 1039m; 1013w; 905w; 868m; 815w; 657w; 551m; 514m; 448w. Raman (on single crystal) (cm^{-1}): 2185s; 1536m; 1400w; 1360m; 1330w; 1290s; 1270s; 1155vs; 555m; 405w; 370w. UV−vis−NIR (reflectance, KBr pellets) λ/nm: 370; 531; 776; 1270.

[Pt(Et$_2$pipdt)$_2$][Pt(mnt)$_2$] (3b). This compound was prepared as described for **3a** (yield 92%), starting from the CH_3CN solutions of $[Pt(Et_2pipdt)_2](BF_4)_2$ (violet; 81 mg; 0.10 mmol) and $(Bu_4N)_2$-$[Pt(mnt)_2]$ (orange; 100 mg; 0.10 mmol). Anal. Calcd for $C_{12}H_{14}N_4$-PtS_4: C, 26.81; H, 2.62; N, 10.45; S, 23.85. Found: C, 26.55; H, 2.68; N, 10.25; S, 24.50%. IR [KBr pellets, cm^{-1}]: 2977vw; 2934vw; 2295vw; 2193vs; 1605w; 1517vs; 1471vs; 1452s; 1353vs; 1299vw; 1271w; 1230s; 1193w; 1149s; 1130s; 1100w; 1042m; 1005vw; 969vw; 870vw; 861m; 793m; 763vw; 672w; 552w; 509m. Raman (on single crystal) (cm^{-1}): 2200w; 1525w; 1478w; 1297vs; 1230m; 1140m; 885vw; 860vw; 550w. UV−vis−NIR (reflectance, KBr pellets) λ/nm: 351; 548; 733; 1072.

[Pd(Me$_2$pipdt)$_2$][Pd(mnt)$_2$] (4a). This compound was prepared as described for **3a** (yield 92%), starting from the CH_3CN solutions of $[Pd(Me_2pipdt)_2](BF_4)_2$ (brown; 71 mg; 0.11 mmol) and $(Bu_4N)_2$-$[Pd(mnt)_2]$ (yellow-green; 100 mg; 0.11 mmol). Crystals suitable for X-ray characterization were grown using a diffusion cell with three compartments as described for **3a**. Anal. Calcd for $C_{10}H_{10}N_4$-PdS_4: C, 28.54; H, 2.39; N, 13.31; S, 30.47. Found: C, 28.14; H, 2.18; N, 13.00; S, 30.10%. IR [KBr pellets, cm^{-1}]: 2993vw; 2279vw; 2247vw; 2179vs; 2140w; 1630vw; 1530vs; 1464vs; 1439vw; 1401m; 1357vs; 1291s; 1264s; 1203m; 1153s; 1138s; 1104s; 1037w; 1011w; 902w; 864w; 813w; 663w; 550m; 514m; 455w. Raman (on single crystal) (cm^{-1}): 2185s; 1540s; 1469s; 1400m; 1360s; 1330m; 1294s; 1270vs; 1158vs; 554w; 336w. UV−vis−NIR (reflectance, KBr pellets) λ/nm: 293; 446; 709; 924.

Measurements. Microanalyses were performed on a Carlo Erba CHNS elemental analyzer model EA1108. IR spectra (4000−200 cm^{-1}) were recorded on KBr pellets with a Perkin Elmer model 983 spectrometer. FT-Raman spectra (resolution 4 cm^{-1}) were recorded on a Bruker RFS100 FT-spectrometer, fitted with an indium-gallium-arsenide detector (room temperature) and operating with an excitation frequency of 1064 nm (Nd:YAG laser). The power level of the laser source varied between 20 and 40 mW. The solid samples were introduced in a capillary tube and then fitted into the compartment designed for a 180° scattering geometry. Raman spectra (2200−300 cm^{-1}) on single crystals were carried out at room temperature using a Raman microscope (BX 40, Olympus) spectrometer (ISA xy 800) equipped with a He−Ne (λ = 632.817 nm, Melles-Griot) laser. A 180° reflective geometry was adopted. The samples were mounted on a glass microscope slide, and the scattering peaks were calibrated against a Si standard (ν = 520 cm^{-1}). Spectra were collected with a 500 s time constant at a 1 cm^{-1} resolution and were averaged over 5 scans. No sample decomposition was observed during the experiments. Electronic spectra (2000−300 nm) were recorded on a Cary 5 spectrophotometer, equipped with a diffuse reflectance accessory (reflectance spectra were recorded on KBr pellets). Cyclic voltammograms were carried out on an EG&G (Princeton Applied Research) potentiostat−galvanostat model 273, using a conventional three-electrode assembly consisting of a platinum wire working electrode, a platinum wire as counter electrode, and a Ag/AgCl reference electrode in saturated KCl solution. The experiments were performed at room temperature (25 °C), in dry and argon-degassed CH_3CN containing 0.1 mol dm^{-3} Bu_4NPF_6 as supporting electrolyte, at a 50−200 mV s^{-1} scan rate. Half-wave potential for the ferrocene/ferrocenium couple (internal standard) is 0.43 V under these conditions. Specific resistivity for **3b**, as compacted pellet, was measured at room conditions by the conventional two-probe method at the Physics Department, University of Cagliari.

Table 1. Crystallographic Data for $[Pt(Me_2pipdt)_2][Pt(mnt)_2]$ (**3a**)

chemical formula	$C_{20}H_{20}N_8Pt_2S_8$
fw	1019.10
space group	$P\bar{1}$ (No. 2)
a (Å)	6.784(7)
b (Å)	8.460(6)
c (Å)	13.510(5)
α (deg)	100.63(2)
β (deg)	104.04(2)
γ (deg)	96.90(2)
V (Å^3)	728.2(10)
Z	1
T (°C)	20
λ(Cu Kα) (Å)	1.541838
D_{calcd} (g cm^{-3})	2.324
μ (cm^{-1})	2.3313
R1 [$I > 2\sigma(I)$][a]	0.0691
wR2 (all data)[b]	0.2187

[a] $R1 = \sum||F_o| - |F_c||/\sum|F_o|$. [b] $wR2 = [\sum w(F_o^2 - F_c^2)^2/\sum wF_o^4]^{1/2}$.

Data Collection and Structure Determination. Diffraction data were collected at room temperature on a Siemens AED diffractometer. The crystallographic data are summarized in Table 1. The lattice parameters were obtained by least-squares analysis of the setting angle of 31 carefully centered reflections chosen from diverse regions of reciprocal spaces in the $18 < \theta < 40°$ range, respectively. The check of one standard reflection during data collection showed no significant decrease. The space group was chosen on the basis of systematic extinction and intensity statistics. The intensities recorded by the $\theta-2\theta$ scan technique were corrected for Lorentz and polarization effects. An absorption correction was applied after the last isotropic refinement cycle following the empirical methods of Walker and Stuart[18] (transmission coefficient: 0.598−1.000). The structures were solved by direct methods through the Sir92[19] program and refined by full-matrix least-squares using the SHELXL-97[20] program with anisotropic thermal parameters for the non-hydrogen atoms. The hydrogen atoms were placed at their geometrically calculated positions and refined using a

(18) Walker, N.; Stuart, D. *Acta Crystallogr*. **1983**, *39A*, 158.
(19) Altomare, A.; Cascarano, C.; Giacovazzo, C.; Guagliardi, A.; Burla, M. C.; Polidori, G.; Camalli, M. *J. Appl. Crystallogr*. **1994**, *27*, 435.
(20) Sheldrick, G. M. *SHELXL-97: Program for Crystal Structure Refinement*; University of Göttingen: Göttingen, Germany, 1997.

Table 2. Bond Lengths [Å] and Angles [deg] for $[Pt(Me_2pipdt)_2][Pt(mnt)_2]$ with esd's

	Cation		
Pt(1)−S(1)	2.290(4)	N(1)−C(5)	1.446(16)
Pt(1)−S(2)	2.264(4)	N(2)−C(2)	1.306(16)
S(1)−C(1)	1.660(14)	N(2)−C(3)	1.461(19)
S(2)−C(2)	1.702(14)	N(2)−C(6)	1.519(18)
N(1)−C(1)	1.322(16)	C(1)−C(2)	1.485(17)
N(1)−C(4)	1.453(18)	C(3)−C(4)	1.509(26)
S(1)−Pt(1)−S(2)	88.69(12)	C(3)−N(2)−C(6)	116.3(12)
S(1)−Pt(1)−S(2′)	91.31(12)	N(1)−C(1)−C(2)	116.8(12)
C(1)−S(1)−Pt(1)	104.8(4)	N(1)−C(1)−S(1)	122.1(10)
C(2)−S(2)−Pt(1)	105.3(4)	C(2)−C(1)−S(1)	121.0(9)
C(1)−N(1)−C(4)	122.8(12)	N(2)−C(2)−C(1)	120.0(12)
C(1)−N(1)−C(5)	118.7(11)	N(2)−C(2)−S(2)	120.8(10)
C(4)−N(1)−C(5)	118.0(11)	C(1)−C(2)−S(2)	119.2(8)
C(2)−N(2)−C(3)	121.3(13)	N(2) −C(3)−C(4)	109.0(13)
C(2)−N(2)−C(6)	121.8(11)	N(1)−C(4)−C(3)	110.8(14)
	Anion:		
Pt(2)−S(3)	2.303(4)	N(4)−C(10)	1.153(23)
Pt(2)−S(4)	2.295(4)	C(7)−C(9)	1.361(20)
S(3)−C(7)	1.727(15)	C(7)−C(8)	1.446(19)
S(4)−C(9)	1.742(14)	C(9)−C(10)	1.432(22)
N(3)−C(8)	1.146(19)		
S(3)−Pt(2)−S(4)	90.14(14)	S(4)−C(9)−C(7)	122.9(11)
S(3)−Pt(2)−S(4″)	89.86(14)	S(4)−C(9)−C(10)	117.0(12)
C(7)−S(3)−Pt(2)	101.9(5)	C(8)−C(7)−C(9)	120.9(13)
C(9)−S(4)−Pt(2)	101.8(5)	C(7)−C(9)−C(10)	120.0(14)
S(3)−C(7)−C(9)	123.2(11)	C(7)−C(8)−N(3)	177.6(17)
S(3)−C(7)−C(8)	115.8(11)	C(9)−C(10)−N(4)	172.5(19)

[a] Symmetry transformations used to generate equivalent atoms: (′) $-x+1, -y, -z$; (″) $-x, -y, -z$.

"riding" model correction on the corresponding carbon atoms. Atomic scattering factors and the anomalous scattering coefficients were taken from *International Tables for X-ray Crystallography*.[21] Bond distances and angles are reported in Table 2. All calculations were carried out on the ENCORE 91 and DIGITAL AlphaStation 255 computers of Parma University.

Results and Discussion

$[M(R_2pipdt)_2](BF_4)_2$ (M = Pd, R = Me; M = Pt, R = Me, Et, Pr^i) Salts. $[M(R_2pipdt)_2](BF_4)_2$ compounds (M = Pd, R = Me; M = Pt, R = Me, Et, Pr^i) have been prepared by reacting *N*,*N*′-dialkyl-piperazine-2,3-dithione (R_2pipdt) dissolved in CH_2Cl_2 with the appropriate metal chloride (2:1 molar ratio). After several hours under reflux, brown solids precipitate. The solids were dissolved in EtOH, and $NaBF_4$ was added to the solutions. The obtained solids have been recrystallized from CH_3CN/Et_2O. Analytical data are in agreement with this formulation, and spectroscopic features are similar to those of the structurally characterized $[Ni(Me_2pipdt)_2](BF_4)_2$[9] and $[Pt(Me_2pipdt)_2](I_3)_2$[22] salts.

In the IR spectra of the complexes, the ν(CN) vibration is shifted by 50−60 cm^{-1} to higher frequencies compared to that of the free ligand, in accordance with an expected increase in the CN double bond character, as a consequence of the coordination through the sulfur atoms. The typical peaks of the BF_4 anions appear as a strong broad peak centered near 1050 cm^{-1} and as a doublet in the 540−520 cm^{-1} range. UV−vis spectra of the corresponding Ni(II), Pd(II), and Pt(II) derivatives are reported in Figure 1. In the visible region, two peaks, whose molar absorptions (Table 3) are too strong to be assigned to d−d transitions, appear. The position of the absorption maxima and the values of the corresponding absorptivities follow the following orders: λ_{max} (Ni > Pt > Pd) and ϵ_{max} (Ni < Pt < Pd). For a better understanding of the nature of these peaks, theoretical calculations based on approximate extended Hückel methods, using the CACAO program,[23] have been performed. Figure 2 shows the frontier orbitals, which are π-type orbitals, for the metal complexes. The contribution of the metals to the frontier empty orbitals is negligible, while their contribution to the frontier populated orbitals is high and affects the energy of these orbitals. In particular, the d_{xz} orbital of Pd gives the highest contribution to the HOMO (d_{xz} Ni 34%; Pd 78%; Pt 55%). The same occurs with d_{yz} in the HOMO − 1 orbital. The peaks in the visible region are assigned to (HOMO − 1)−LUMO and HOMO−LUMO transitions, and the composition of these orbitals (the occupied MOs have a metal as well as a ligand character, while the LUMO is virtually a pure ligand orbital) agrees with the different contribution of the three metal d_{yz} and d_{xz} orbitals to the HOMO − 1 and HOMO. In fact, the decreasing contribution of metal d orbitals in the order Pd > Pt > Ni can explain the decrease in the HOMO − 1 and HOMO stabilization

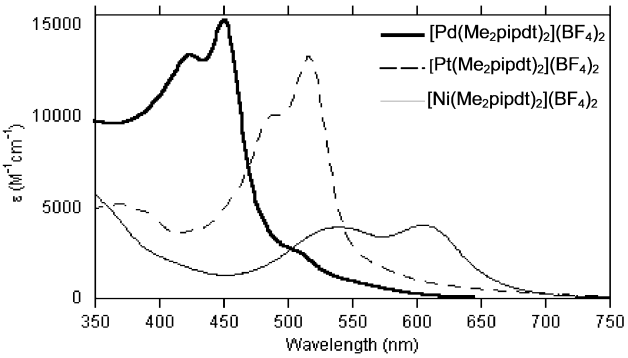

Figure 1. UV−vis spectra of $[M(Me_2pipdt)_2](BF_4)_2$ salts in CH_3CN solution.

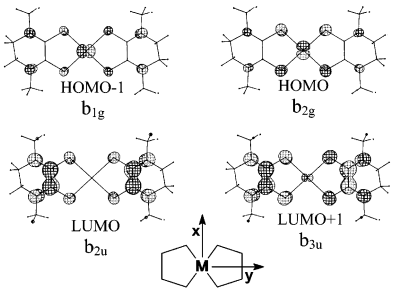

Figure 2. Frontier MOs of $[M(Me_2pipdt)_2]^{2+}$.

Table 3. Visible Absorptions and Molecular Density of $[M(Me_2pipdt)_2](BF_4)_2$

complex	λ_1 (nm)	ϵ_1 (M^{-1} cm^{-1})	λ_2 (nm)	ϵ_2 (M^{-1} cm^{-1})
$[Ni(Me_2pipdt)_2](BF_4)_2$	540	4000	605	4000
$[Pd(Me_2pipdt)_2](BF_4)_2$	424	13400	450	15200
$[Pt(Me_2pipdt)_2](BF_4)_2$	489	sh	516	13300

(21) *International Tables for X-ray Crystallography*; Kynoch Press: Birmingham, England, 1974; Vol. IV, pp 99−102 and 149.
(22) Bigoli, F.; Deplano, P.; Mercuri, M. L.; Pellinghelli, M. A.; Pintus, G.; Serpe, A.; Trogu, E. F. *J. Am. Chem. Soc.* **2001**, *123*, 1788.
(23) Mealli, C.; Proserpio, D. *J. Chem. Educ.* **1990**, *67*, 39.

Scheme 1

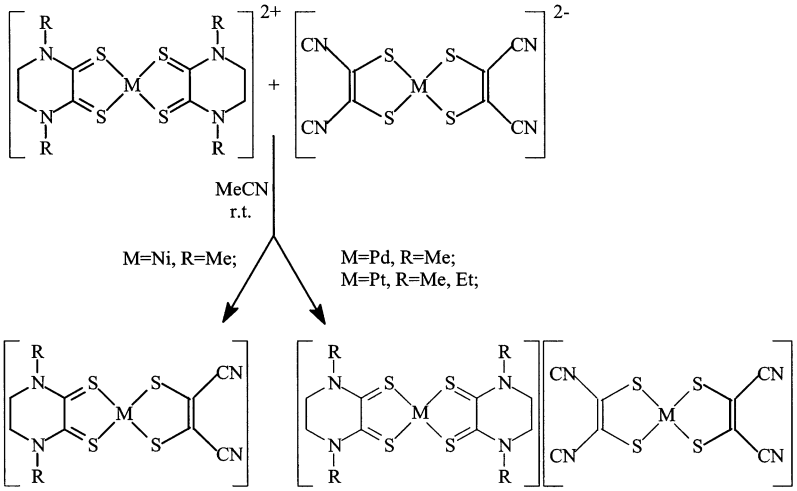

Table 4. Cyclic Voltammetry

complex	$E_{1/2}$[a] (V)			
$[Ni(Me_2pipdt)_2](BF_4)_2$	−0.16	−0.41	−0.96	−1.26
$[Pd(Me_2pipdt)_2](BF_4)_2$	−0.18	−0.42	−0.87	−1.13
$[Pt(Me_2pipdt)_2](BF_4)_2$	−0.15	−0.41	−0.92	−1.21

[a] Measured at Pt electrodes in CH_3CN solutions, 0.1 M Bu_4NPF_6 supporting electrolyte at 100 mV s^{-1} scan rate. Reference electrode Ag/AgCl in saturated KCl.

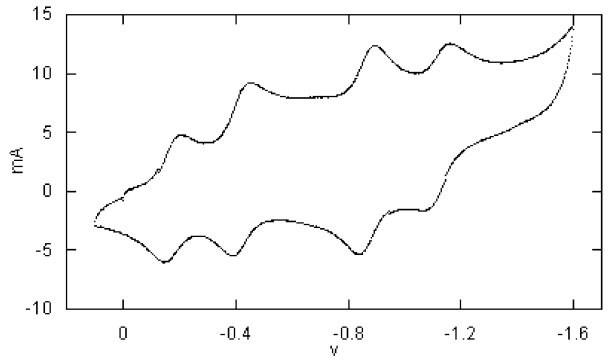

Figure 3. Cyclic voltammetry of $[Pd(Me_2pipdt)_2](BF_4)_2$ between 0.2 and −1.6 V.

and in the CT (metal to ligand) contribution to the (HOMO − 1)−LUMO and HOMO−LUMO transitions, thus explaining the energy and intensity sequence of the low energy transitions on varying the metal. These findings also agree with the results of cyclic voltammograms (CVs). The CVs (Table 4 and see Figure 3 as an example of the $[Pd(Me_2pipdt)_2](BF_4)_2$ case) exhibit four reversible redox steps which can be ascribed to the following processes:

$$[M(Me_2pipdt)_2]^{2+} \overset{E_{1/2}^1,\ 1e^-}{\rightleftharpoons} [M(Me_2pipdt)_2]^{+} \overset{E_{1/2}^2,\ 1e^-}{\rightleftharpoons} [M(Me_2pipdt)_2] \overset{E_{1/2}^3,\ 1e^-}{\rightleftharpoons} [M(Me_2pipdt)_2]^{-} \overset{E_{1/2}^4,\ 1e^-}{\rightleftharpoons} [M(Me_2pipdt)_2]^{2-}$$

The $E_{1/2}$ values for the reduction processes are very similar for the different metal complexes, those related to the E^1 and E^2 processes in particular, further supporting the fact that the contribution of the metals to the involved orbital (LUMO) is negligible.

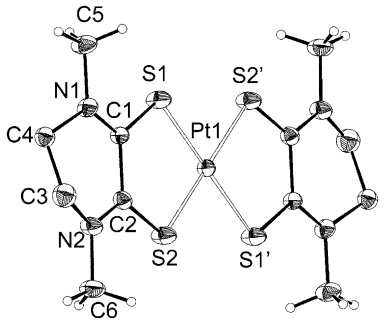

Figure 4. Perspective view of the cation $[Pt(Me_2pipdt)_2]^{2+}$ of $[Pt(Me_2pipdt)_2][Pt(mnt)_2]$. Thermal ellipsoids are drawn at the 30% probability level.

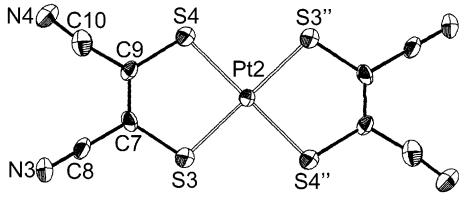

Figure 5. Perspective view of the anion $[Pt(mnt)_2]^{2-}$ of $[Pt(Me_2pipdt)_2][Pt(mnt)_2]$. Thermal ellipsoids are drawn at the 30% probability level.

$[M(Me_2pipdt)_2][M(mnt)_2]$ (M = Pd, R = Me; M = Pt, R = Me, Et). As shown in Scheme 1, the reaction between $[M(R_2pipdt)_2](BF_4)_2$ and $(Bu_4N)_2[M(mnt)_2]$ produces the mixed-ligand complex $[Ni(R_2pipdt)(mnt)]$ for M = Ni and R = Me quantitatively, while for M = Pd, R = Me and M = Pt, R = Me or Et, the $[M(R_2pipdt)_2][M(mnt)_2]$ double salts are formed by metathesis.

The Pt salt, R = Me (**3a**), has been structurally characterized, and the crystallographic data are summarized in Table 1. Structural data show that approximately square-planar $[Pt(Me_2pipdt)_2]$ dications and regular square-planar $[Pt(mnt)_2]$ dianions are present. The molecular structures of the cation and the anion, along with the atomic labeling scheme, are shown in Figures 4 and 5, respectively. An infinite anion−cation one-dimensional stack along the *a* axis with a Pt···Pt *a*/2 distance of 3.392 Å (see Figures 6 and 7), and a Pt···Pt···Pt angle of 180° is formed. Anions and cations

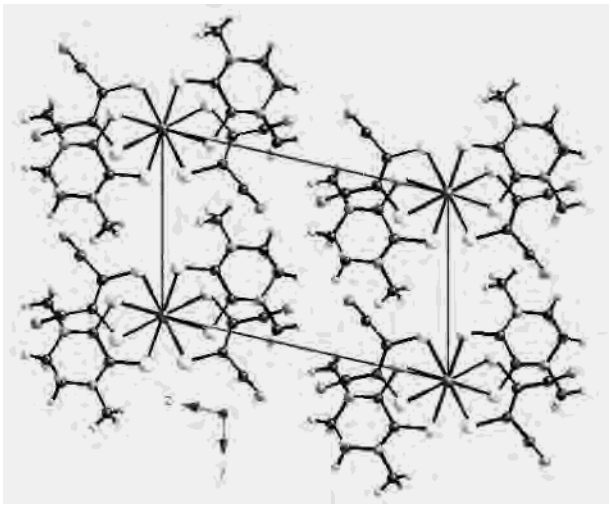

Figure 6. Projection of $[Pt(Me_2pipdt)_2][Pt(mnt)_2]$ along *a*.

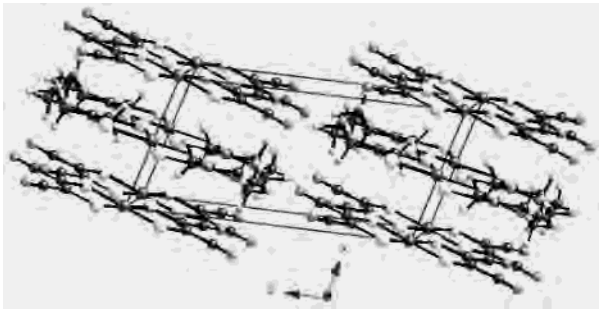

Figure 7. Crystal structure of $[Pt(Me_2pipdt)_2][Pt(mnt)_2]$ as viewed along *b*.

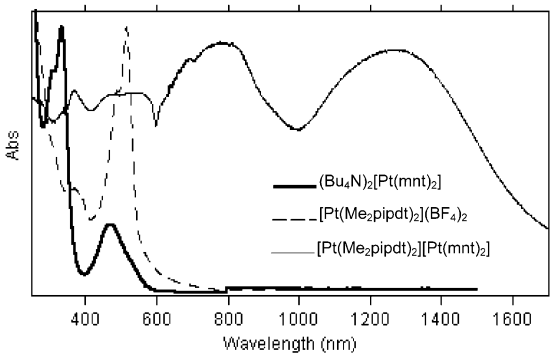

Figure 8. Diffuse reflectance spectra of $[Pt(Me_2pipdt)_2][Pt(mnt)_2]$ and, for comparison, the CH_3CN solution spectra of $[Pt(Me_2pipdt)_2](BF_4)_2$ and $(Bu_4N)_2[Pt(mnt)_2]$. The absorbances are reported in arbitrary units.

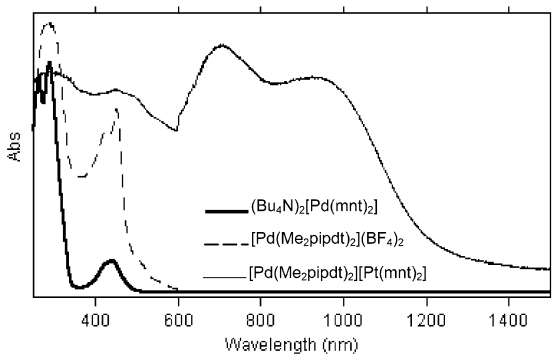

Figure 9. Diffuse reflectance spectra of $[Pd(Me_2pipdt)_2][Pd(mnt)_2]$ and, for comparison, the CH_3CN solution spectra of $[Pd(Me_2pipdt)_2](BF_4)_2$ and $(Bu_4N)_2[Pd(mnt)_2]$. The absorbances are reported in arbitrary units.

arrange themselves face-to-face in such a way as to result in a staggered orientation. The ions of each species lie on alternating planes parallel to *bc*. The most significant bond distances and angles are reported in Table 2. The structural features within the $[Pt(Me_2pipdt)_2]$ cation agree with those found in the triiodide salt[22] of this cation. Moreover, bond distances and angles of the square-planar anions $[Pt(mnt)_2]^{2-}$ are consistent with those found in the crystal structures of its tetraethyl[24] and *n*-butylammonium salts.[25] The structural features of the stacked salt agree well with those of $[Pt(CNMe)_4][Pt(mnt)_2]$, where a similar infinite anion−cation staggered stacking with Pt···Pt distance of 3.328 Å is found.[26]

The reflectance spectra of $[M(Me_2pipdt)_2][M(mnt)_2]$ (and, for comparison, solution spectra of the components) are reported in Figures 8 and 9 for M = Pt and Pd, respectively. Two strong broad bands appear at 776 and 1270 nm (Pt salt), and at 709 and 924 nm (Pd salt). One-dimensional complexes formed by the stacking of square-planar tetracyanoplatinate (and bisoxalatoplatinates) show absorption bands in the visible region, which are assigned to transitions between the bands formed by the overlap of the platinum d_{z^2} and p_z orbitals (Pt···Pt distances below 3 Å).[27] Because the Pt···Pt distances for this class of one-dimensional Pt salts are too long (∼3.4 Å) to allow a significant overlap of the previously cited Pt orbitals, similar assignments of the observed near-IR absorptions cannot be invoked.[28] As cited in the Introduction, the nickel mixed-ligand complexes show two bands at low energy, and the one at the lower energy exhibits strong negative solvatochromism. This absorption has been assigned to an intramolecular charge transfer (ICT) transition between the HOMO and the LUMO, where the ligand with electron-withdrawing substituents (mnt, dmit) gives a prevailing contribution to the HOMO, while the ligand with electron-donating substituents (R_2pipdt) gives a prevailing contribution to the LUMO. The complexes are describable as dithione−dithiolate derivatives where an intramolecular ligand-to-ligand charge-transfer transition (from the dithiolate to the dithione ligand) gives rise to a strong absorption at low energies. In the case of Pd and Pt derivatives, dithione and dithiolate are coordinated in separate complexes which form a salt where an outer-sphere ligand-to-ligand transition from the negatively charged to the positively charged complex may be responsible for the observed long-wavelength transition. A similar outer-sphere ligand-to-ligand charge-transfer assignment has been made to explain the absorption band

(24) Clemenson, P. I.; Underhill, A. E.; Hursthouse, M. B.; Short, R. L. *J. Chem. Soc., Dalton. Trans.* **1989**, 61.
(25) Guntner, W.; Gliemann, G.; Klement, U.; Zabel, M. *Inorg. Chim. Acta* **1989**, *165*, 51.
(26) Bois, H.; Connelly, N. G.; Crossley, J.; Guillorit, J.-C.; Lewis, G. R.; Orpen, A. G.; Thornton, P. *J. Chem. Soc., Dalton. Trans.* **1998**, 2833.
(27) Williams, J. M. *Adv. Inorg. Chem. Radiochem.* **1983**, *26*, 235.
(28) The difference between the orbitals involved in intrachain overlap in platinum tetracyanoplatinate (or bisoxalatoplatinates) (d_{z^2} and p_z orbitals) and those involved in platinum-dithiolenes (ligand π-system) has also been observed in one-dimensional metals based on the described anions. See: Ahmad, M. M.; Turner, D. J.; Underhill, A. E.; Kobayashi, A.; Sasaki, Y.; Kobayashi, H. *J. Chem. Soc., Dalton Trans.* **1984**, 1759.

Table 5. Reduction Potentials of Component Ions, Free Reaction and Activation Enthalpies of Electron Transfer between Ions, and Ion Pair Charge-Transfer Band of Solid Ion Pairs

$[M(R_2pipdt)_2][M(mnt)_2]$	E ($C^{2+/+}$) (V)	E ($A^{-/2-}$) (V)	E_{IPCT} (eV)	ΔG_{12} (eV)	ΔG^* (eV)
M = Pt; R = Me	−0.13	+0.21	0.976	+0.34	0.37
M = Pt; R = Et	−0.17	+0.21	1.159	+0.37	0.43
M = Pd; R = Me	−0.16	+0.46	1.342	+0.62	0.62

of [Ni(tim)][Ni(mnt)$_2$] (tim = 2,3,9,10-tetramethyl-1,4,8,-11-tetra-azacyclotetradeca-1,3,8,10-tetraene), whose structure, however, is unknown.[29] An extensive investigation on several ion pair charge-transfer (IPCT) complexes formed by dianionic dithiolene metalates (A) and organic dications consisting of 4,4′- and 2,2′-bipyridinium (C) derivatives has been performed by Kisch.[15] Also in these salts which exhibit a strong absorption in the visible−near-infrared region, both components are redox-active and undergo reversible electron transfers in the ground state. Using the Hush−Marcus model,[30] Kisch has shown that the relation between optical and thermal electron transfer is followed by several salts formed by dianionic dithiolene metalates and organic dications, previously cited, when both components are planar and form a mixed donor−acceptor stack in the solid state. When solution measurements are not available, the following modified Hush relation, which relates the energy of the CT transition to the driving force of electron transfer $[C]^{2+} + [A]^{2-} \rightarrow [C]^{+} + [A]^{-}$, is proposed:

$$E_{IPCT} = \chi + \Delta G_{12} \quad (1)$$

[E_{IPCT} is obtained from the IPCT peak in the reflectance spectra, χ represents the total reorganization energy, and ΔG_{12} is obtained from the components' redox potential difference, $E(C^{2+/+}) - E(A^{-/2-})$.] Moreover, the free activation enthalpy of the thermal electron transfer can be calculated according to the following:

$$\Delta G^* = E^2_{IPCT}/4(E_{IPCT} - \Delta G_{12}) \quad (2)$$

The expected linear correlation between E_{IPCT} and ΔG_{12} was satisfactorily followed by several dianionic dithiolene metalates and organic dications of the type C[M(mnt)$_2$] and C[M(dmit)$_2$]. Measurements of electrical specific conductivity gave values ranging from 10^{-10} to 10^{-3} Ω^{-1} cm^{-1}, and these values are related to ΔG_{12} and ΔG^*. This relationship furnishes a tool to design molecular materials whose electrical conductivity may be controlled by the proper choice of components. Our findings are in very good agreement with Kisch's results, when the organic cations are changed by the redox-active metallo-dithiolene cations $C^{2+} = [M(R_2pipdt)_2]^{2+}$. The E_{IPCT}, ΔG_{12}, and ΔG^* values obtained for $[M(R_2pipdt)_2][M(mnt)_2]$ (M = Pd, R = Me and M = Pt, R = Me, Et, see Table 5) fall in the range reported for salts formed by the dianionic dithiolene metalates, based on mnt and dmit ligands, and 4,4′- or 2,2′-bipyridinium dications (C), and the plot of E_{IPCT} versus ΔG_{12} shows the expected linear decrease in the energy of the CT transition with increasing driving force of the thermal electron transfer. Though the used number of points is very low, the plot of E_{IPCT} versus ΔG_{12} has a slope of 1.1 in good agreement with the 1.0 theoretical value and an intercept (the mean reorganization energy) of 0.66 eV in surprisingly good agreement with the 0.63 eV value, which was found when the data on several dithiolene-metalate−viologen ion pairs were taken into account. Moreover, a room-temperature electrical specific conductivity of pressed powder pellets of $[Pt(Et_2pipdt)_2][Pt(mnt)_2]$ has been determined in accordance with the expected value [$\sigma = (1.2 \pm 0.5)10^{-7}$ Ω^{-1} cm^{-1}] on the basis of the log σ linear dependence on ΔG_{12} and ΔG^*. On the whole, the results agree with an ion pair charge-transfer description for the salts $[M(R_2pipdt)_2][M(mnt)_2]$ (M = Pd, R = Me; M = Pt, R = Me, Et), where the CT band is assigned to a transition from the dithiolene metalate donor to the dicationic dithiolene acceptor $\pi \rightarrow \pi^*$ ($b_{2g} \rightarrow b_{2u}$, see MOs reported for $[M(mnt)_2]^{2-}$ in ref 31, and frontier orbitals for $[M(Me_2pipdt)_2]^{2+}$ in Figure 2). The similarity of $[M(R_2pipdt)_2][M(mnt)_2]_2$ (M = Pd, R = Me; M = Pt, R = Me, Et) salts to C[Ni(mnt)$_2$] can be explained by taking into account the nature of the LUMO of the organic acceptor and the LUMO of $[M(Me_2pipdt)_2]^{2+}$, which is also a π^* ligand orbital (see electrochemical and theoretical calculation results on the previously described dications). In the present case, an additional absorption which is absent in the reflectance spectra of the cation and anion precursor salts is found at low energies. Tentatively, this band may be ascribed to another ILCT $\pi \rightarrow \pi^*$ ($b_{1u} \rightarrow b_{3g}$) transition, but an intramolecular $\pi \rightarrow \pi^*$ transition of $[M(mnt)_2]^{2-}$ (M = Pd, Pt), where a stabilization of the π^* orbitals of suitable (a_u) symmetry possibly produced by interaction with 5 or $6p_z$ (M = Pd, Pt) orbitals, cannot be ruled out, and theoretical studies are required for more reliable assignments.

Vibrational studies have been performed to correlate the charge of mnt complexes[32] with the position of the C=C stretch. This peak is found at 1485 cm^{-1} for $[M(mnt)_2]^{2-}$ and at 1435 cm^{-1} for $[M(mnt)_2]^{-}$. In $[M(Me_2pipdt)_2][M(mnt)_2]$ salts (M = Pd, Pt), the peaks assigned to the ν(CN) vibration of the cations and the ν(C=C) of the anions are found at lower frequencies compared to the corresponding vibrations of the dication in the BF_4 salt and of the dianion in the R_4N salt (but higher than of the monoanions, see Table 6). These findings agree with a small amount of charge delocalization between the donor and the acceptor in $[M(Me_2pipdt)_2][M(mnt)_2]$ charge-transfer complexes, although the observed shifts of ν(CN) and ν(C=C) do not strictly correlate with ΔG_{12}.

Conclusions

New salts of the redox-active dithiolene cations $[M(R_2pipdt)_2]^{2+}$ have been shown to be valuable reagents for

(29) Vogler, A.; Kunkely, H. *J. Chem. Soc., Chem. Commun.* **1986**, 1616.
(30) Hush, N. S. *Prog. Inorg. Chem.* **1967**, *8*, 391. Marcus, R. A.; Sutin, N. *Comments Inorg. Chem.* **1986**, *5*, 119.
(31) Guntner, W.; Gliemann, G. *J. Phys. Chem.* **1990**, *94*, 618.
(32) Schläpfer, C. W.; Nakamoto, K. *Inorg. Chem.* **1975**, *14*, 1338. Wootton, J. L.; Zink, J. I. *J. Phys. Chem.* **1995**, *99*, 7251. Kutsumizu, S.; Kojima, N.; Ban, T.; Tsujikawa, I. *Bull. Chem. Soc. Jpn.* **1987**, *60*, 2547−2553.

Table 6. Most Significant IR Peaks[a]

	ν(C=C)[b] cm^{-1}	ν(CN) cm^{-1}
Me_2pipdt		1500
$Na_2[Ni(mnt)_2]$	1485	
$Na[Ni(mnt)_2]$	1435	
$[Pd(Me_2pipdt)_2](BF_4)_2$		1553
$(n\text{-}Bu_4N)_2[Pd(mnt)_2]$	1482	
$[Pd(Me_2pipdt)_2][Pd(mnt)_2]$	1460	1530
$[Pt(Me_2pipdt)_2](BF_4)_2$		1550
$(n\text{-}Bu_4N)_2[Pt(mnt)_2]$	1480	
$[Pt(Me_2pipdt)_2][Pt(mnt)_2]$	1460	1538
$K[Pt(mnt)_2]$	1422−1396 (br)	

[a] Spectra recorded on KBr pellets. [b] Assigned following references quoted in ref 32.

preparing complexes of interest in material chemistry. For M = Ni, R = Me, their reaction with $[M(mnt)_2]^{2-}$ dianionic dithiolenes produces $[Ni(Me_2pipdt)(mnt)]$ mixed-ligand derivatives, which are potential second-order nonlinear chromophores showing strong negative solvatochromism and β. For M = Pd, R = Me and M = Pt, R = Me or Et, ion pair charge-transfer salts made up of an infinite mixed planar anion−cation one-dimensional stack are produced. The CT interactions strongly affect their properties and depend on the redox properties of the components. By applying the "Marcus−Hush model", a linear correlation between thermal transition and optical electron transition, similar to the one reported earlier for stacked salts of the same dianionic dithiolene metalates with planar organic dications, is found for the salts described here which represent an example of fully inorganic CT complexes. Because the planarity of the components is a crucial requirement for obtaining charge-transfer semiconducting salts, these cationic metal-dithiolene complexes, in which the planarity of the central core is maintained by the d^8-metal atom (which imposes square-planar geometry) while the ligand may be properly modified, are very versatile and seem promising in preparing new charge-transfer salts where the redox potential of the molecular components can be tuned on a wider range.

Acknowledgment. The authors are grateful to Dr. S. Sanna, Physics Department, Cagliari University, for specific conductivity measurements. This work has been developed in the framework of European COST action D14 "Towards New Molecular Inorganic Conductors".

Supporting Information Available: Table of crystal data, structure solution and refinement, atomic coordinates, bond lengths, angles, and anisotropic thermal parameters for **3a** (CIF). This material is available free of charge via the Internet at http://pubs.acs.org.

IC025788W